RASĀYAN *J. Chem.*
Vol. 19 | No. 4 | 2424-2431 | October-December | 2026
ISSN: 0974-1496 | e-ISSN: 0976-0083 | CODEN: RJCABP
http://www.rasayanjournal.com
http://www.rasayanjournal.co.in

OPTIMIZATION OF A BITUMEN-POLYMER-ZNO COATING FOR ENHANCED MECHANICAL STRENGTH AND CORROSION RESISTANCE

G. B. Temirov[1,✉], F. M. Yusupov[1], A.R. Qurbonov[1], S. U. Khalilov[1], S. B. Sultonov[1], S. S. Rakhimjonova[2], and N.A. Ismailova[2]

[1]The Institute of General and Inorganic Chemistry of the Academy of Sciences of the Republic of Uzbekistan, Tashkent, 100071, Uzbekistan

[2]Tasheknt institute of Chemical Technology, 100011, Tashkent, Uzbekistan

✉Corresponding author: temirovgolib1995@gmail.com

ABSTRACT

Corrosion remains a critical challenge in industrial environments, necessitating the development of durable and cost-effective protective coatings. In this study, composite anticorrosion coatings based on modified bitumen-polymer systems were formulated and evaluated. The optimal composition (C5) consisted of 25 wt% bitumen, 30 wt% urethane-alkyd binder, 30 wt% pyrolysis distillate, 10 wt% microcalcite, and 5 wt% ZnO. Mechanical, thermal, and electrochemical performances were systematically investigated. C5 exhibited the highest microhardness of 635 $HV_{0.1}$ at 12 V compared to 620 $HV_{0.1}$ for the control sample (AM). Temperature-dependent analysis showed that drying time decreased from 28-18 h at -10 ºC to 8-4.5 h at 50-60 °C, with C4-C5 demonstrating the fastest curing behaviour. Conditional tensile strength increased up to 0.22 at 20 °C for C5 and remained higher than AM (0.20) across the investigated range, maintaining 0.15 at 60 °C. Electrochemical testing revealed significant improvement at 12 V, where E_{corr} shifted to -200 mV, Icorr decreased to 1.24μA·cm^{-2}, the corrosion rate dropped to 15.1μm·year^{-1}, and polarisation resistance reached 21.6 kΩ·cm^2. The results confirm that the optimised C5 formulation provides enhanced mechanical stability, accelerated curing, and superior corrosion resistance, making it a promising solution for long-term protection of industrial metal structures.

Keywords: Anti-Corrosion Coatings, Mechanical Strength, Drying Time, Microhardness, Corrosion Resistance

RASĀYAN *J. Chem.*, Vol. 19, No.4, 2026

INTRODUCTION

Metal structures, pipelines, and storage tanks widely used in industrial and construction sectors are continuously exposed to corrosion due to the influence of moisture, oxygen, saline solutions, and aggressive chemical environments.[1] These processes lead to a deterioration of mechanical strength, a reduction in service life[2], and significant economic losses. Therefore, the development of effective and long-term corrosion protection methods for metal surfaces remains one of the most important and urgent challenges in modern materials science.[3] One of the most effective approaches to corrosion protection is the application of various coating materials.[4,5] Although conventional epoxy and polymer-based coatings exhibit high protective efficiency, many of them are characterised by complex synthesis procedures, high production costs, and environmental limitations.[6] Moreover, recent studies emphasise that corrosion resistance is determined not only by the mechanical strength of a coating but also by its continuity, hydrophobicity, and adhesion to the metal substrate, which are considered key factors governing long-term protection performance.[7] Bitumen-based mastics possess significant practical potential as anticorrosion materials due to their excellent water impermeability[8], strong adhesion, and stability in aggressive environments. The inherent hydrophobic nature of bitumen enables it to act as an effective barrier that restricts the penetration of oxygen and electrolytes to the metal surface.[9] However, coatings based on unmodified bitumen are prone to ageing-related hardening, sensitivity to temperature fluctuations, and limited mechanical durability. Consequently, there is a clear need to modify the composition of bitumen mastics and to investigate their structure-property relationships on a scientific basis.[10] Recent research has demonstrated that the effectiveness of anticorrosion coatings is governed not only by the presence of additives or inhibitors but also by coating density, molecular-level interactions, and mechanisms associated with the formation of passive barrier layers.[11] In particular, materials capable

http://doi.org/10.31788/RJC.2026.1949795
This work is licensed under a CC BY 4.0 license.

of forming continuous, non-porous, and highly hydrophobic films have been shown to exhibit superior corrosion resistance even under aggressive environmental conditions.[12,13] This approach is equally relevant for bitumen mastics, indicating that optimisation of their composition and processing conditions can lead to a substantial improvement in anticorrosion performance.[14,15] However, limited information is available on the combined influence of urethane-alkyd binder, pyrolysis distillate, microcalcite, and ZnO on the mechanical and electrochemical performance of bitumen-based anticorrosion coatings. In particular, the relationship between coating composition, deposition voltage, microhardness, curing behaviour, and corrosion resistance has not been systematically established. Therefore, the present study aims to optimise a bitumen-polymer-ZnO coating formulation and evaluate its physicochemical, mechanical, and electrochemical properties.

EXPERIMENITAL

Materials

In this study, a 60/90 penetration grade road bitumen was used as the primary binder for the preparation of anticorrosion bitumen mastic. The bitumen was produced at the Bukhara Oil Refinery in accordance with GOST 22245-90 and was selected due to its balanced penetration value, adequate softening point, strong adhesion, and high-water impermeability. These characteristics ensure structural stability and durability of the protective coating system (Table-1).

Table-1: List of Individual Raw Materials and their Basic Physical Properties

Materials	Code	SG (G_s)	BD (kg/m^3)	Pen (25 ◦C)	SP (◦C)	RV (135 ◦C) (mPa.s)	BET SA (m^2 /g)	% passing 90 μm
60/90 bitumen	BND	1.01-1.06	-	62	47	443.2	-	-
Pyrolysis distillate	PD	1.10	-	*	62	845.4	-	-
Alkyd lacquer	Al	0.9-1.05	-	**	**	**	-	-
Micro calcite	MC	2.72	1520	-	-	-	3.72	100
Zink oxide	ZO	5.6	520	-	-	-	9.12	99.8

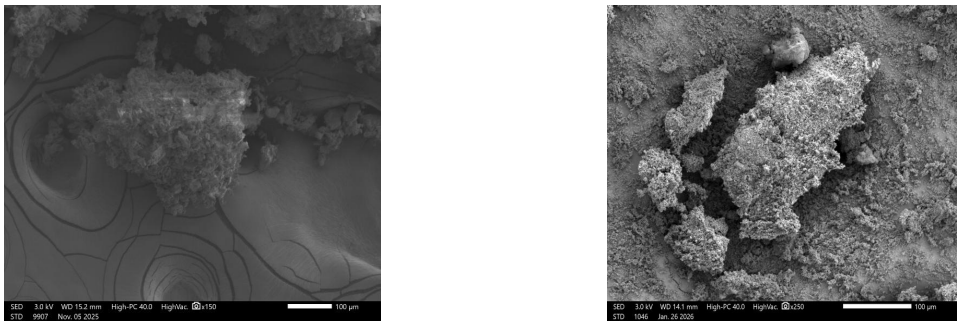
*Test was not conducted due to high data variability and equipment limitations.
** Properties supplied by the material manufacturer.

A urethane-alkyd varnish (Hayat) was used as a polymer modifier to enhance elasticity, flexibility, and adhesion of the binder. Urethane segments improve crack resistance under thermal and mechanical stress, while the alkyd component promotes adhesion to metal substrates and supports film formation. Its compatibility with hydrocarbon systems ensures uniform dispersion in the bitumen matrix (Table-1). Heavy pyrolysis oil was added as a plasticiser and viscosity modifier, reducing system viscosity, improving processability, and minimising low-temperature brittleness due to decreased internal stresses. Its hydrocarbon nature ensures good compatibility with bitumen and improved rheological behaviour. Zinc oxide (ZnO, Asl Kimyo) was incorporated as an active anticorrosion additive. It provides surface passivation, reduces electrochemical corrosion, and enhances resistance to ageing and aggressive environments. Its distribution within the coating was analysed by SEM/EDS (Fig.-1). Microcalcite ($CaCO_3$) was introduced as a mineral filler to enhance density, structural integrity, and mechanical strength of the mastic. The effectiveness of microcalcite is closely related to its fine particle size and surface characteristics. SEM analysis confirmed uniform particle morphology and satisfactory dispersion within the coating structure (Fig.-1), promoting the formation of a dense and homogeneous protective layer.

Physical Properties of Raw Materials

To evaluate the physical properties of the raw materials used in this study, a set of key parameters was investigated. These included the specific gravity (SG, Gs), bulk density (BD, kg/m^3), penetration at 25 °C (Pen), softening point (SP, °C), rotational viscosity at 135 °C (RV, mPa·s), specific surface area (BET SA, m^2/g), and the percentage passing the 90 μm sieve (% passing 90 μm).

These parameters provide a basis for assessing the processability, structural stability, and performance-related properties of the raw materials within the bitumen mastic system. The obtained results are presented in Table-2.



(a) (b)

Fig.-1: SEM images of Microcalcite ($CaCO_3$) and Zinc Oxide (ZnO) at 100 µm (overall morphology) and 20 µm (particle structure and aggregation)

Table-2: Quantitative Ratios of Components in the Prepared Bitumen Mastic Compositions

Materials	Code	Mass fraction (%)
Control sample (Aqua Mast)	AM	100%
Composition-1	C1	BND (50 %) + Al (25 %) + PD (10 %) + MC (15 %) + ZO (0 %)
Composition-2	C2	BND (40 %) + Al (25 %) + PD (15 %) + MC (20 %) + ZO (0 %)
Composition-3	C3	BND (35 %) + Al (25 %) + PD (20 %) + MC (15 %) + ZO (0 %)
Composition-4	C4	BND (30 %) + Al (30 %) + PD (25 %) + MC (10 %) + ZO (5 %)
Composition-5	C5	BND (25 %) + Al (30 %) + PD (30 %) + MC (10 %) + ZO (5 %)

Preparation of Anti-Corrosion Bitumen Mastic

In order to assess the effect of individual components on anticorrosion bitumen mastic performance, one control sample (neat bitumen) and five modified formulations were prepared. Microcalcite was ground and sieved to <90 µm prior to use. The bitumen was heated to a molten state, followed by the addition of urethane-alkyd varnish and heavy pyrolysis oil under continuous stirring. Microcalcite was gradually incorporated to avoid agglomeration, while ZnO was added at the final stage to ensure uniform dispersion. The mixture was stirred until homogeneous and stored in sealed containers before testing.

Characterization Techniques

FTIR spectra were recorded using a Spectrum Two (PerkinElmer) spectrometer in ATR mode (4000-400 cm^{-1}) to identify functional groups and possible interactions among components. Surface morphology and filler dispersion were examined by SEM, while elemental composition and ZnO distribution were analysed by EDS (point and mapping modes). Corrosion resistance was evaluated by immersion of coated substrates in 3 wt.% NaCl solution, with corrosion rate determined from mass loss measurements. Mechanical properties (tensile strength and adhesion) were measured using a universal testing machine, and drying time was defined as the period required to reach a non-tacky state. Coatings of the control (AM) and modified samples (C1-C5) were also prepared using a laboratory jet electrodeposition system with controlled temperature, electrolyte circulation, DC power supply, and a rectangular nozzle to ensure uniform deposition.

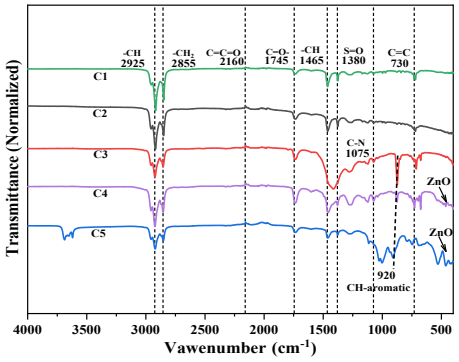
RESULTS AND DISCUSSION

FTIR analysis was performed on the five initially prepared samples (C1-C5). The obtained spectral results were used to identify the presence of functional groups and to evaluate the compositional differences among the samples. The results are presented in Fig.-2.

According to Fig.-2, the bands at 2925 and 2855 cm^{-1} correspond to asymmetric and symmetric stretching of -CH and $-CH_2$ groups, confirming the presence of long aliphatic chains from bitumen and pyrolysis distillate. The strong peak at 1745 cm^{-1} is assigned to C=O stretching of ester groups from the urethane–alkyd lacquer, with higher intensity in C4 and C5 due to increased lacquer content.

Peaks at 1465, 730, and 920 cm^{-1} indicate C-H deformation, C=C stretching, and aromatic C-H vibrations, while the band at 1075 cm^{-1} confirms C-N stretching associated with urethane groups. The absorption at 1380 cm^{-1} corresponds to S=O vibrations from sulfur-containing compounds, and the weak band at 2160

cm^{-1} suggests partial chemical modification of the matrix. In C4 and C5, the band at 470 cm^{-1} confirms Zn-O vibrations, verifying the incorporation of ZnO and its passivating role.

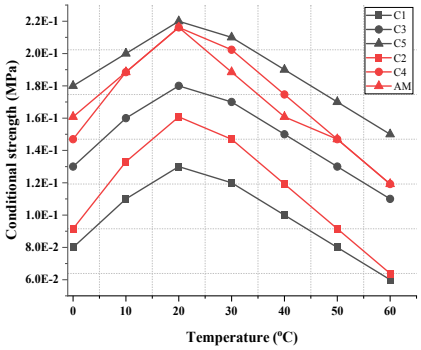


(a)

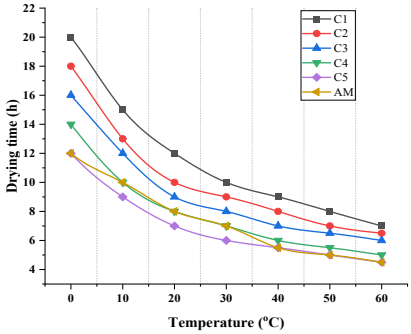
Wavenumber cm^{-1}	Functional group
470	ZnO
730	C=C-alkene
920	C-H-Aromatic
1075	C-N-Aromatic amine
1380	S=O - Sulfuric
1465	C-H alkene
1745	C=O- esters
2160	C=C=O-ketene
2855	CH_2-alkane

(b)

Fig.-2: Comparative FTIR Spectra of the Synthesized Samples (C1-C5)



(a)



(b)

Fig.-3: Effect of Temperature on the Conditional Strength (a) and Drying Time (b) of Anticorrosion Coatings (C1-C5 and AM)

Temperature-dependent evaluation of drying time and conditional strength highlights the strong influence of formulation on coating performance. As temperature increases from −10 to 60 °C, the drying time of all samples (C1-C5 and AM) progressively decreases. At −10 °C, drying time ranges from 28 h (C1) to 18 h (C5 and AM), while at 50-60 °C it declines to 8-7 h for C1 and 5-4.5 h for C5 and AM. Throughout the entire range, C4 and C5 show consistently shorter drying times than C1-C3, indicating that higher polymer and plasticiser contents accelerate film formation.

In contrast, conditional tensile strength increases from -10 °C to about 20 °C and then gradually decreases at higher temperatures. For instance, C5 rises from 0.14 at -10 °C to 0.22 at 20 °C, then drops to 0.15 at 60 °C. Similar trends are observed for other samples (C1 peak 0.13; C4 and AM up to 0.20). C5 maintains the highest strength across the full temperature range, while C4 shows comparable but slightly lower values. The decline above 20 °C is attributed to thermal softening of the bitumen-polymer matrix. Notably, at 60 °C C5 combines rapid drying (4.5 h) with relatively high strength (0.15), outperforming AM (0.13), confirming the balanced performance of the optimised C5 formulation.

Figure-4 illustrates the variation of microhardness of the coatings (C1-C5 and AM) as a function of jet voltage. For all samples, a similar trend is observed: the microhardness increases with increasing jet voltage, reaches a maximum value at an intermediate voltage (around 6-20 V), and then gradually decreases at higher voltages.

This behaviour indicates the existence of an optimal jet voltage range for achieving dense and mechanically robust coatings. Among the modified coatings, samples C1-C4 exhibit moderate increases in microhardness, with their peak values ranging between approximately 590 and 630 HV_{01}. In contrast, sample C5 demonstrates the highest microhardness over the entire voltage range, reaching a maximum value of about 635 HV_{01} at 12 V, which is significantly higher than those of the other compositions and the control sample (AM).

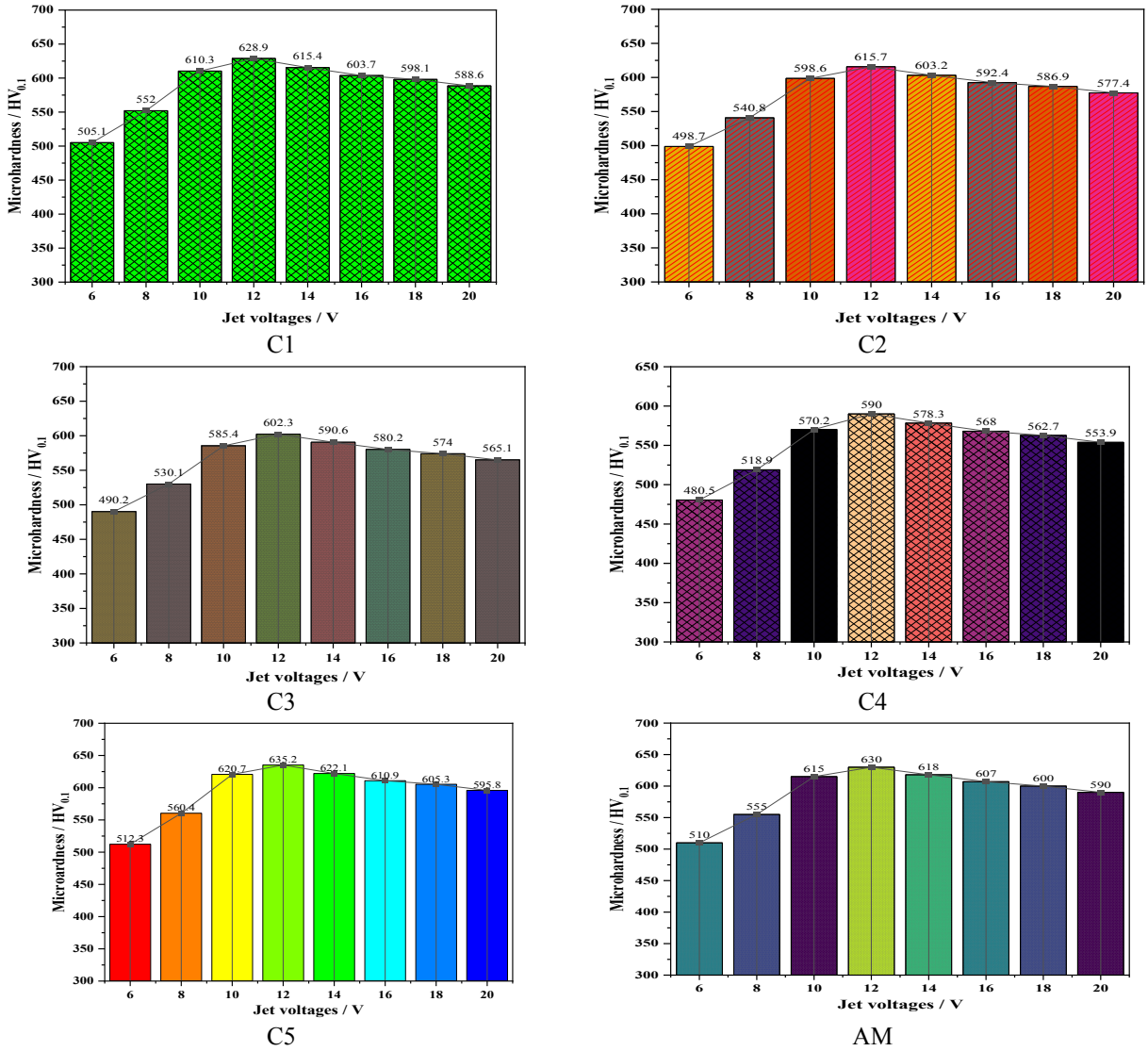


Fig.-4: Microhardness of Coatings (C1-C5 and AM) as a Function of Jet Voltages

The superior microhardness of C5 can be attributed to the optimal balance between the polymer-modified bitumen matrix, pyrolysis distillate, mineral filler, and ZnO additive. In the subsequent stage of the study, the corrosion properties of the selected C5 sample were investigated. The obtained results are summarised in Table- 3.

Table-3: Corrosion Characteristics of C5

Jet Voltage (V)	Ecorr (mV)	Icorr (μA·cm^{-2})	Corrosion Rate (μm·year^{-1})	βa (mV/dec)	βc (mV/dec)	Rp (kΩ·cm^2)
6	-582	32.80	398.2	405	345	2.65
8	-481	8.40	101.4	211	509	7.85
10	-413	1.85	22.4	70	733	14.60
12	-200	1.24	15.1	86	388	21.60
14	-305	2.00	21.5	230	170	18.20
16	-225	2.70	31.6	78	460	9.20
18	-290	8.50	103.0	160	700	6.00
20	-500	10.50	127.0	230	280	4.70

The electrochemical parameters of the C5 coating (Table-3) strongly depend on jet voltage. At 6 V, poor protection is observed (Ecorr = -582 mV, Icorr = 32.80 μA·cm^{-2}, corrosion rate = 398.2 μm·year^{-1}),

indicating insufficient coating compactness. Increasing the voltage to 12 V significantly enhances performance: Ecorr shifts to -200 mV, Icorr decreases to 1.24 μA·cm^{-2}, the corrosion rate drops to 15.1 μm·year^{-1}, and Rp reaches 21.60 kΩ·cm^2, confirming formation of a dense protective layer. At voltages above 12 V, corrosion resistance deteriorates (Icorr up to 10.50 μA·cm^{-2}; corrosion rate up to 127.0 μm·year^{-1}. Rp down to 4.70 kΩ·cm^2), likely due to defects from excessive deposition rates. Changes in βa and βc values further suggest voltage-dependent reaction kinetics, with higher βc at intermediate voltages indicating effective cathodic suppression. In the next stage of the study, EDS analysis was performed on the optimal C5 composition in order to investigate the spatial distribution of elements and to determine whether any elemental agglomeration occurred during the mixing process. Results are shown in Fig.-5.

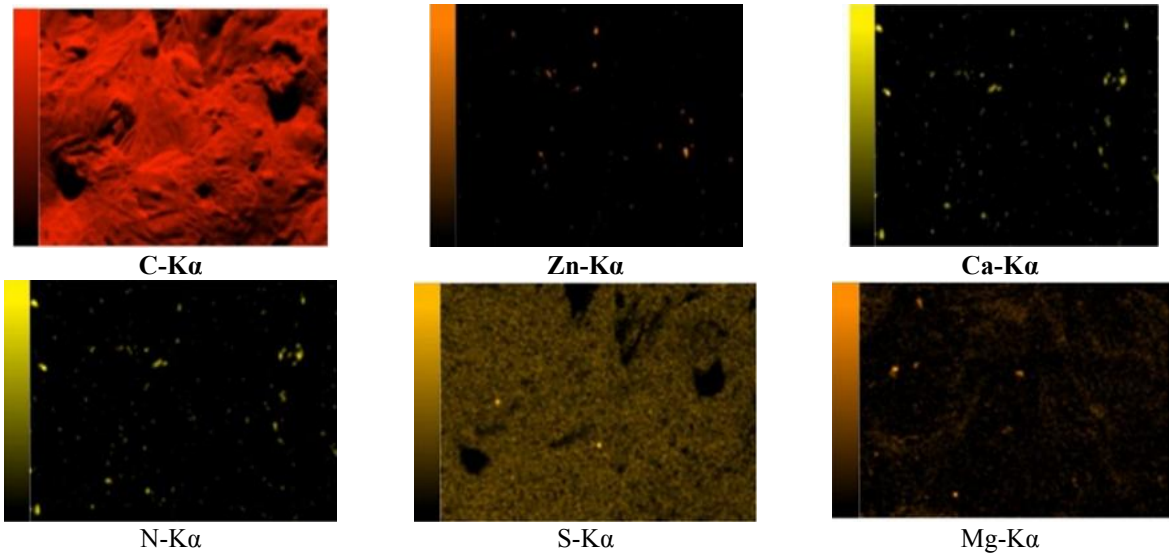


Fig.-5: EDS Elemental Mapping Analysis of the C5 Coating Exhibiting the Highest Corrosion Protection Performance

C-Kα mapping shows a high and uniform carbon distribution, confirming the formation of a continuous organic-polymeric matrix that acts as an effective barrier against corrosive species. Zn-Kα indicates finely and homogeneously dispersed zinc, contributing to cathodic protection and surface passivation. Ca-Kα reveals evenly distributed calcium from mineral fillers, enhancing coating density and mechanical stability. N-Kα suggests the presence of nitrogen-containing functional groups that promote adsorption-based corrosion inhibition. S-Kα demonstrates uniform sulfur distribution, supporting passive layer formation on the metal surface. Mg-Kα, although low in intensity, reflects its stabilising role in improving thermal and chemical resistance. Overall, the homogeneous elemental distribution in C5 confirms its structural integrity and the synergistic contribution of barrier, passivation, and inhibition mechanisms to superior anticorrosion performance.

CONCLUSION

This study confirmed that modification of bitumen mastics with urethane–alkyd varnish, pyrolysis distillate, microcalcite, and ZnO significantly enhances mechanical and anticorrosion performance compared to the control sample (AM). The optimal formulation C5 (25 wt% bitumen, 30 wt% urethane–alkyd binder, 30 wt% pyrolysis distillate, 10 wt% microcalcite, and 5 wt% ZnO) demonstrated the highest microhardness of 635 HV0.1 at 12 V (AM: 620 HV0.1). Temperature-dependent analysis showed that drying time decreased from 28–18 h at −10 °C to 8–4.5 h at 50–60 °C, with C4–C5 exhibiting the fastest curing behaviour. Conditional tensile strength reached a maximum of 0.22 at 20 °C for C5 (AM: 0.20) and remained higher across the entire temperature range, maintaining 0.15 at 60 °C (AM: 0.13). Electrochemical testing further revealed that at 12 V, Ecorr shifted to -200 mV, Icorr decreased to 1.24 μA·cm^{-2}, the corrosion rate dropped to 15.1 μm·year^{-1} (from 398.2 μm·year^{-1} at 6 V), and Rp reached 21.6 kΩ·cm^2. Future studies should include long-term salt-spray and weathering tests, adhesion durability, scale-up, and field validation. By potentially extending the service life of metallic infrastructure and

reducing maintenance and replacement requirements, this study contributes to United Nations Sustainable Development Goal-9: Industry, Innovation and Infrastructure.

ACKNOWLEDGMENTS

The authors express their sincere gratitude to the Institute of General and Inorganic Chemistry of the Academy of Sciences of the Republic of Uzbekistan for providing the laboratory facilities, instrumental and equipment support, and scientific guidance that made this research possible.

CONFLICT OF INTERESTS

The authors declare no conflict of interest.

AUTHOR CONTRIBUTIONS

The present work is related to *SDG-9: Industry, Innovation and Infrastructure*. All the authors contributed significantly to this manuscript, participated in reviewing/editing and approved the final draft for publication. The research profile of the authors can be verified from their ORCID ids, given below:

G.B. Temirov https://orcid.org/0009-0000-2064-1938
F.M. Yusupov https://orcid.org/0000-0002-6758-3445
A.R. Qurbonov https://orcid.org/0009-0005-1896-8081
S.U. Khalilov https://orcid.org/0009-0007-9458-3268
S.B. Sultonov https://orcid.org/0000-0003-1996-1744
N.A. Ismailova https://orcid.org/0000-0003-2543-9442
S.S. Rakhimjanova https://orcid.org/0000-0002-6163-5988

Open Access: This article is distributed under the terms of the Creative Commons Attribution 4.0 International License (http://creativecommons.org/licenses/by/4.0/), which permits unrestricted use, distribution, and reproduction in any medium, provided you give appropriate credit to the original author(s) and the source, provide a link to the Creative Commons license, and indicate if changes were made.
Cite this article as: G. B. Temirov *et al.*, *Rasayan J. Chem.*, 19(4), 2424-2431(2026), https://doi.org/10.31788/RJC.2026.1949795

REFERENCES

1. J. Zhou, Q. Zhang, R. Liu, J. Luo, *Progress in Organic Coatings,* **211,** 109831(2026), https://doi.org/10.1016/j.porgcoat.2025.109831
2. D. Zhou, Z. Zhu, X. Ruan, C.-A. Xu, Y. Hu, *International Journal of Biological Macromolecules,* **335,** 149296(2026), https://doi.org/10.1016/j.ijbiomac.2025.149296
3. Y. Jiahao, L. Jun, L. Yujun, Q. Jiangpeng, Z. Jing, M. Jiliang, *Optics and Laser Technology,* **196,** 114625(2026), https://doi.org/10.1016/j.optlastec.2025.114625
4. C. Che, T. Greenfield, M. Wang, B. Zhang, *Progress in Organic Coatings,* **213,** 109979(2026), https://doi.org/10.1016/j.porgcoat.2026.109979
5. Q. Guo, Y. Zheng, J. Zhang, *Progress in Organic Coatings,* **213,** 109977(2026), https://doi.org/10.1016/j.porgcoat.2026.109977
6. Y. Lv, Q. Luo, G. Gu, Y. Li, W. Sun, M. Liu, M. Yue, M. Fei, *Surfaces and Interfaces,* **78,** 108100(2025), https://doi.org/10.1016/j.surfin.2025.108100
7. S. Han, C. Ke, Y. Wu, B. Yu, X. Wang, Y. Bo, W. Xianzong, W. Long, L. Dongsheng, F. Zhou, L. Liu, *Progress in Organic Coatings,* **213,** 109952(2026), https://doi.org/10.1016/j.porgcoat.2026.109952
8. L. Shupei, G. Feng, S. Huanhuan, Y. K. Yunlong, W. Changhao, Z. Yuxin, *Chemical Engineering Journal,* **526,** 170608(2026), https://doi.org/10.1016/j.cej.2025.170608
9. S. Zhang, Q. Shi, J. Li, Y. Ren, J. Zhao, *Colloids and Surfaces A: Physicochemical and Engineering Aspects*, **736,** 139641(2026), https://doi.org/10.1016/j.colsurfa.2026.139641
10. G. B. Temirov, F. M. Yusupov, S. K. Yusupov, G. A. Baymatova, A. A. Kucharov, N. Yodgorov, D. Z. Nuriddinova, *Rasayan Journal of Chemistry,* **18(4)**, 2225(2025), https://doi.org/10.31788/RJC.2025.1849355

11. Y. Cai, Z. Cheng, J. Zhao, B. He, B. Yang, Sh. Anding, J. Pujun, *Materials Chemistry and Physics,* **350,** 131939(2026), https://doi.org/10.1016/j.matchemphys.2025.131939
12. S. Liu, H. Zhou, L. Wan, Y. Chen, X. Zhang, *Progress in Organic Coatings,* **211,** 109828(2026), https://doi.org/10.1016/j.porgcoat.2025.109828
13. H. Chen, M. Xu, J. Wang, C. Li, X. Liu, M. Wu, W. Wei, L. Longmin, L. Yongzhao, W. Yu, Y. Lai, W. Cai, *Surface and Coatings Technology,* **519,** 132987(2026), https://doi.org/10.1016/j.surfcoat.2025.132987
14. F. Gao, Y. Wang, S. She, R. Zhu, Y. Wang, Z. Liang, *Chemical Engineering Journal,* **528,** 172165(2026), https://doi.org/10.1016/j.cej.2025.172165
15. J. Su, Y. Zhang, P. Huang, H. Wen, *Colloids and Surfaces A: Physicochemical and Engineering Aspects*, **728,** 138596(2026), https://doi.org/10.1016/j.colsurfa.2025.138596

[RJC-9795/2026]